This is the peer reviewed author accepted manuscript (post print) version of a published work that appeared in final form in:

Oppong, Francis, Luo, Zhongyang, Li, Xiaolu, Song, Yang, Xu, Cangsu, Lacina Diaby, Abdullatif 2022 'Laminar combustion characteristics of ethyl acetate/hydrogen/air at elevated pressures', Fuel, vol. 330, article no. 125631, pp. 1-13

This output may not exactly replicate the final published authoritative version for which the publisher owns copyright. It is not the copy of record. This output may be used for non-commercial purposes. This version is licensed under a Creative Commons CC-BY-NC-ND 4.0 license (http://creativecommons.org/licenses/by-nc-nd/4.0/).

The final definitive published version (version of record) is available at: https://doi.org/10.1016/j.fuel.2022.125631

Persistent link to the UniSA Research Outputs Repository: https://researchoutputs.unisa.edu.au/11541.2/30388

General Rights

Copyright and moral rights for the publications made accessible in the UniSA Research Outputs Repository are retained by the authors and/or other copyright owners and it is a condition of accessing publications that users recognize and abide by the legal requirements associated with these rights.

- Users may download and print one copy for the purpose of private study or research.
- You may not further distribute the material or use it for any profit-making activity or commercial gain
- You may freely distribute the persistent link identifying the publication in the UniSA Research Outputs Repository

If you believe that this document breaches copyright, please contact us and provide details. We will remove access to the work immediately and investigate your claim.

Laminar combustion characteristics of ethyl acetate/hydrogen/air at elevated pressures

Francis Oppong[a], Zhongyang Luo[a], Xiaolu Li[b], Yang Song[c], Cangsu Xu[a*], Abdullatif Lacina Diaby[d]

[a]College of Energy Engineering, State Key Laboratory of Clean Energy Utilization, Zhejiang University, Hangzhou, 310027, China P.R.

[b]College of Mechanical and Electrical Engineering, China Jiliang University, Hangzhou, 310018, China P.R.

[c]Zhejiang Tongji Vocational College of Science and Technology, Hangzhou, 311231, China P.R.

[d]UniSA Online (STEM), University of South Australia, Adelaide, SA 5000, Australia.

*Corresponding author: xucangsu@zju.edu.cn

Abstract

Ethyl acetate/hydrogen/air (EA/H_2/air) premixed flame combustion characteristics were investigated at the initial pressures of 1 bar, 2 bar, and 3 bar and a temperature of 358 K using H_2 in air volumetric fractions of 0%, 4%, 8%, and 12%. Specifically, the laminar burning speed (LBS) and intrinsic flame instabilities of the EA/H_2/air premixed flames were investigated. The laminar burning speed follows the order of 0% < 4% < 8% < 12%. The maximum laminar burning speeds of 0.85 m/s, 0.78 m/s and 0.70 m/s were measured at the initial pressures of 1, 2 and 3 bar, respectively, when a 12% concentration of hydrogen was added to EA. EA/H_2/air LBS was significantly promoted and inhibited by reactions R98: $H + O_2 \Leftrightarrow O + OH$ and R136: $CH_3 + H (+M) \Leftrightarrow CH_4 (+M)$, respectively. Furthermore, decreased flame thickness or curvature effect mainly caused the instability and cellularity of the EA/H_2/air premixed flames when the concentration of hydrogen and the initial pressure increased. EA/H_2/air premixed flames were thermal-diffusively stable and hydrodynamically unstable. This study provides a profound understanding of the combustion characteristics of EA/H_2/air relevant to its application in combustors.

Keywords: Ethyl acetate (EA); Hydrogen (H_2); Expanding spherical flame; Laminar burning speed; Intrinsic instabilities

1. Introduction

The combustion of fossil fuels in energy conversion devices and/or combustors has been identified as one of the primary human-caused sources of CO_2 emissions and a contributor to global warming. Therefore, in the quest to keep global warming at 2°C or even 1.5°C, different green energy reform frameworks have been explored and considered. Ethyl acetate (EA) and hydrogen (H_2) are promising alternative energy carriers to fossil fuels due to their potential to reduce greenhouse gas (GHG) emissions. EA is a biomass-based energy carrier that has desirable physicochemical characteristics such as non-hygroscopy, high octane rating, high heat of combustion, etc. that make it an attractive fuel or fuel additive in internal combustion engines (ICEs) [1,2]. Compared to ethanol, EA has better water tolerance and can be mixed with gasoline without adverse effects like phase separation and changing the vapour pressure of the fuel mixture [3,4]. On the contrary, EA has a slower or delayed ignition rate than ethanol [5]. Similarly, H_2 is a carbon-free fuel with a wide range of flammability limits and a high burning speed [6,7]. Moreover, blending H_2 with hydrocarbon/oxygenated fuels could influence the reactivity and diffusivity of the fuel mixture [8,9]. That is, blending H_2 with hydrocarbon fuels could reduce fuel consumption and enhance the lean burning limit of the fuel mixture, increase the burning speed, and decrease the combustion duration of the premixture [7,10]. In this regard, it is noteworthy to investigate the effect of hydrogen on oxygenated fuels like EA and the possibility of using both fuels as a mixed transportation fuel to reduce engine-out emissions without compromising ICE performance. Therefore, insight into the combustion characteristics and/or chemistry of EA/H_2/air in ICEs is worth investigating.

Laminar burning speed (LBS) is very significant in energy conversion equipment or combustion devices. LBS is the normal velocity of the unburnt mixture with respect to a planar flame front [11]. Therefore, LBS characterizes the propagation of a flame into a quiescent unburned mixture ahead of the flame at a particular pressure and temperature. LBS embodies the reactivity, diffusivity and exothermicity of a premixed flame [12,13]. LBS can be used to evaluate flame extinction, blow-off, flame stability, etc. [14]. Moreover, LBS can be used to determine the turbulent burning speed and validate the chemical kinetics mechanism of fuels [15]. LBS can also be used to improve the combustion phasing of spark-ignition engines and decrease their knocking tendency, thereby enhancing the engine output torque or power [16]. On the one hand, premixed flames are characterized by intrinsic instabilities that influence the performance of ICEs'. Intrinsic instabilities increase the burning rate of premixed flames and enhance ICEs efficiency and output power;

albeit, they could cause undesirable ICEs performance [17]. In this context, it is important to understand the LBS, intrinsic instability, and chemical reactions of EA/H_2/air premixture for their effective and clean use in ICEs.

Thus far, Refs. [2,18–21] investigated EA's laminar combustion characteristics, and their findings indicated that irrespective of EA's potential as a future transportation fuel, it has low LBS. In a different study, Xu et al. [22] added hydrogen to EA to analyse its LBS at 1 bar and 358 K which is inadequate to give deeper insight into the combustion of EA/H_2/air. However, EA/H_2/air mixture combustion characteristics like LBS and intrinsic flame instability have to be widely studied at different pressures. The motivation of this study is to provide noteworthy information on the laminar burning characteristics of EA/H_2/air premixed flame including, LBS, intrinsic instability, and chemical kinetics, which can be used to further investigate EA/H_2/air fuel mixture combustion for its viable application in ICEs. To this end, this study aims to provide a considerable understanding of EA/H_2/air premixed flame LBS and intrinsic instabilities at an initial temperature of 358 K and initial pressures of 1, 2, and 3 bar. Following the objective of this study, 0%, 4%, 8%, and 12% volumetric fractions of H_2 in air were mixed with EA to study the laminar flame characteristics of the premixture. The constant volume method (CVM) of the spherically expanding flame method was used to study the LBS of EA/H_2/air premixed flames.

2. Experimental investigations

The experimental combustion rig used in this study consists of a constant volume combustion chamber (CVCC) with an internal size of 2.067 L equipped with 0.105 m diameter translucent quartz windows on its sides. The test rig also has an imaging unit which consists of a Schlieren image set up with a high-speed camera (Phantom v2512: 30 000 fps @ 512 × 512 pixels) used to snap the flame images. The combustion vessel was heated by heating elements mounted on the sides of the vessel, and a K-type thermocouple (± 0.75%) was used to measure the initial temperature. The in-chamber and initial pressures were recorded by a pressure sensor (0.0001 MPa resolution) and a high precision digital pressure gauge, respectively. The fuel mixture was ignited with two centrally positioned electrodes (diameter = 0.4 mm) and an ignition module. The ignition energy of the experiment is 15 mJ. A schematic of the experimental rig can be found in Ref. [23]. The test was performed at the initial pressures of 1, 2, and 3 bar and an initial temperature of 358 K using H_2 in a compressed air volumetric fraction of 0%, 4%, 8%, and 12% added to EA. The volumetric

fraction of H_2/air was monitored by a mass flow meter (HORIBA METRON S500). The combustion reactions for stoichiometric EA and H_2 are given in Equations (1) and (2), respectively.

$$C_4H_8O_2 + 5(O_2 + 3.76N_2) = 4CO_2 + 4H_2O + 18.8N_2 \quad (1)$$

$$H_2 + 0.5(O_2 + 3.76N_2) = H_2O + 1.88N_2 \quad (2)$$

Equation (3) was used to determine the mixture's global equivalence ratio (ϕ):

$$\chi_{EA}C_4H_8O_2 + \chi_{H_2}H_2 + \left(\frac{5}{\phi}\chi_{EA} + \frac{\chi_{H_2}}{2\phi}\right)(O_2 + 3.76N_2) \quad (3)$$

$$\chi_{H_2} = \frac{V_{H_2}}{V_{H_2} + V_{air} + V_{EA}} \quad (4)$$

$$\chi_{EA} = 1 - \chi_{H_2} \quad (5)$$

where V_{H_2}, V_{air}, and V_{EA} refers to the volumes of hydrogen, air, and EA respectively. Before the combustion experiment, the combustion chamber was filled with H_2/air for 5 minutes to clean the CVCC. Afterwards, the chamber was vacuumed to almost 0.30 bar absolute pressure and heated to 358 K. Then, EA was injected into the chamber using 100 µL to 1 mL micro syringes and allowed to settle (vaporize) for 5 minutes. Next, H_2/air mixture was injected into the chamber. Prior to ignition of the EA/H_2/air mixture, the mixture was given 3 minutes to mix homogeneously. The experimental uncertainty was due to the initial temperature (ΔU_T^2), initial pressure (ΔU_p^2), fuel measurements (ΔU_f^2), and the combustion chamber volume (ΔU_c^2). The uncertainty was determined using the square roots of the sum of the squares method, $\sqrt{\Delta U_T^2 + \Delta U_p^2 + \Delta U_f^2 + \Delta U_c^2}$ which was estimated to be around $\pm$ 2.03%. ΔU_T^2, ΔU_p^2, ΔU_F^2, and ΔU_V^2 are respectively given as 0.75%, 0.15%, 2.53%, 0.7%. The experimental uncertainties are presented using the 95% confidence interval in the form of error bars to deal with unforeseen errors.

3. Data processing and computational analysis

The filtered experimental pressure data was processed using Equation (6) which was also used to calculate the combustion pressure (p). Afterwards, Equation (7) was used to determine the burnt mass fraction (x) of the combustion process. Equations (7) and (8) were introduced into Equation (10) to determine the stretched laminar burning speed (S_L). Extrapolation was used to calculate the unstretched laminar burning speed (S_L^0) at the initial conditions (see Equation (11)).

$$p = 0.49346(V - V_i) + p_i \tag{6}$$

The burnt mass fraction (x) of the combustion phenomena is computed as [24]:

$$x = \frac{p - p_i f(p)}{p_{max} - p_i f(p)} \tag{7}$$

$$\frac{dx}{dp} = \frac{1 - p_i f'(p)}{p_{max} - p_i f(p)} + \frac{p_i f'(p)[p - p_i f(p)]}{[p_{max} - p_i f(p)]^2} \tag{8}$$

$$p_i f'(p) = \left(\frac{\gamma_u - \gamma_b}{\gamma_u}\right)\left(\frac{p}{p_i}\right)^{-1/\gamma_u} \tag{9}$$

The stretched LBS (S_L) is determined as [25]:

$$S_L = \frac{R_v}{3}\left(1 - (1 - x)\left(\frac{p_i}{p}\right)^{1/\gamma_u}\right)^{-2/3}\left(\frac{p_i}{p}\right)^{1/\gamma_u}\frac{dp}{dt}\frac{dx}{dp} \tag{10}$$

The unstretched LBS (S_L^0) can be evaluated using:

$$S_L = S_L^0(p_r)^a \tag{11}$$

p_i and p_{max} are the initial and maximum pressures respectively; p_r is the pressure ratio p/p_i; V and V_i are voltage and initial voltage respectively; R_v is the combustion vessel inner radius; correspondingly, γ_u and γ_b

are the unburnt and burnt gas specific heat ratios. a is a constant. Considering stretch and heat loss effects in the CVCC fitting range of $1.5 \leq (p_r) \leq 2.5$ was used for the extrapolations of the LBS [26,27]. It is worth noting that the constant volume method (CVM) of the spherically expanding flame method was used to determine the LBS. Figure 1a presents an example of the processed experimental pressure data obtained with Equation (2). As depicted in the figure, the pressure rises after ignition and obtains the peak pressure due to the increased combustion reaction rate. Afterwards, the pressure decreases due to heat loss in the CVCC. The plot shows that the peak pressure of the combustion process is higher at ϕ of 1.23 due to the increased thermal energy of the combustion process. Furthermore, Figure 1b shows the flame speed curve at ϕ of 0.82 obtained with the pressure data in Figure 1a. It is important to mention that similar pressure and flame speed curves can be obtained for the other experimental conditions. However, the results might not be the same, but the trend will be similar. Moreover, the CVCC is formed by the intersection of three orthogonal cylinders, the pressure change in the CVCC is equivalent to that in a spherical chamber.

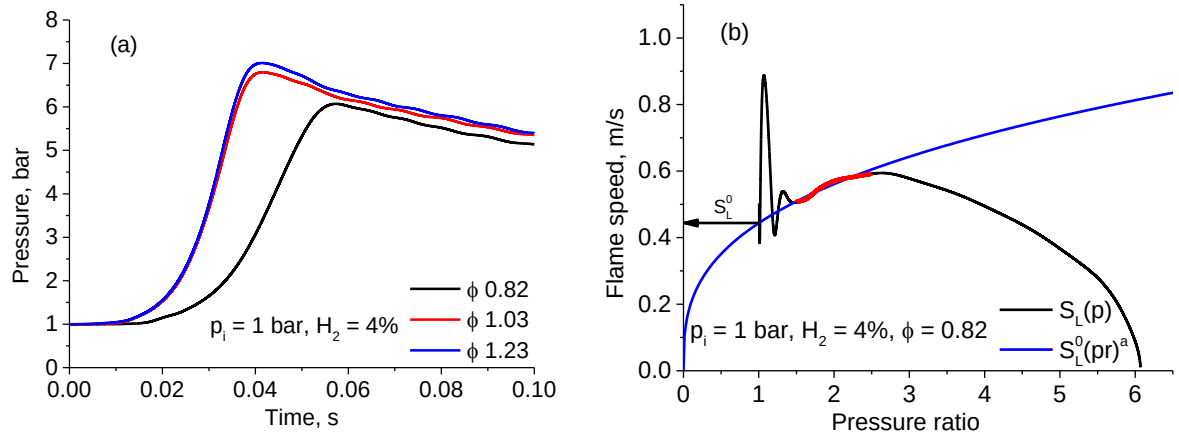


Fig. 1. EA/H_2/air (a) pressure traces and (b) flame speed curve. In Fig. 1b, the fitting range of $1.5 \leq (p_r) \leq 2.5$ is marked with red colour (represents 5646 experimental data points).

The computational analysis involves the calculation of the adiabatic flame temperature, volumetric heat release rate, combustion maximum pressure, thermal diffusivity, Lewis number, flame thickness, thermal expansion ratio, rate of progress, reaction pathways, etc. These parameters were determined using Cantera thermochemical software [28] and the EA chemical mechanism proposed by Ahmed et al. [20]. The Ahmed et al. mechanism is based on the kinetic mechanism for alkane combustion and provides a satisfactory understanding of small esters such as EA combustion chemistry. The 1D freely propagating flame in Cantera

was used to compute the simulated LBS. The computational conditions for the LBS simulations are width = 0.03 m, ratio = 3, slope = 0.06, and curve = 0.12. The grid width is automatically adapted to determine the accurate solution. The Lewis number (Le_f) of the fuel is determined from Equation (12).

$$Le_f = \left[\frac{\chi_{EA}}{Le_{EA}} + \frac{\chi_{H_2}}{Le_{H_2}}\right]^{-1} \quad (12)$$

From Equation (13), the effective Lewis number (Le_{eff}) of the fuel and oxidizer is computed [29,30]:

$$Le_{eff} = 1 + \big((Le_E - 1) + (Le_D - 1)A\big)/(1 + A) \quad (13)$$

Using Equation (14), the flame thickness (δ) can be determined [31]:

$$\delta = (T_a - T_{in})/(dT/dx)_{max} \quad (14)$$

The thermal expansion ratio is calculated using Equation (15) [32].

$$\sigma = \rho_u/\rho_b \quad (15)$$

where A is the mixture strength defined as:$1 + \beta(\varphi - 1)$. φ is the ratio of excess to deficient reactant in the premixture; φ = 1/ϕ for lean mixtures and φ = ϕ for rich mixtures. Le_E, Le_D, χ_{H_2}, χ_{EA}, and β are the Lewis number of excess reactants, deficient reactants, the mole fraction of H_2, the mole fraction of EA, and Zel'dovich number, respectively. Le_{H_2} and Le_{EA} are the Lewis numbers of H_2 and EA, respectively. T_a, T_{in}, and $(dT/dx)_{max}$ are the adiabatic flame temperature, initial temperature, and maximum temperature gradient, respectively. ρ_u and ρ_b represent the unburnt and burnt mixture densities, respectively.

4. Results and discussion

4.1. EA/H_2/air adiabatic flame temperature, thermal diffusivity, and heat release rate

Herein, EA/H_2/air premixed flame adiabatic flame temperature, thermal diffusivity, and the volumetric heat release rate determined with the Cantera thermochemical software are presented and discussed. The adiabatic

flame temperature represents the thermodynamics of a premixed flame. It affects the combustion intensity or reaction rate, the heat released during the combustion process, and the LBS of a premixed flame [33]. Figure 2a shows the adiabatic flame temperatures of EA/H_2/air premixed flame at different H_2 concentrations and the initial pressure of 1 bar. As presented in Figure 2a, irrespective of the equivalence ratio, the adiabatic flame temperature of the EA/H_2/air premixture increases with the increasing concentration of H_2 in the fuel mixture due to an increased chemical reaction rate. Akin to the adiabatic flame temperature, the thermal diffusivity of a premixed flame impacts the reactivity and the LBS of a premixed flame [34]. Figure 2b indicates that the thermal diffusivity of the EA/H_2/air premixed flame increases when the concentration of H_2 in the premixture increases. In a nutshell, EA/H_2/air adiabatic flame temperature and thermal diffusivity data show that the LBS of the EA/H_2/air premixed flame increases when the concentration of H_2 in the premixture increases.

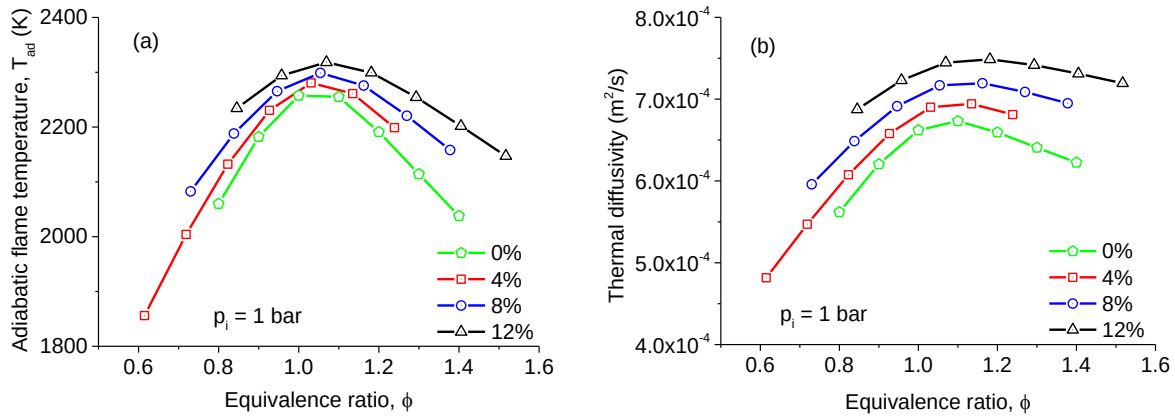


Fig. 2. EA/H_2/air premixed flame (a) adiabatic flame temperature and (b) thermal diffusivity at 1 bar for H_2 of 0-12%.

The rate of heat released from the combustion process of a fuel mixture is important to determine the performance of internal combustion engines or systems. The heat release rate embodies the amount of energy generated from the combustion process. Hence, a deeper understanding of the heat release rate is vital for the design and optimization of combustion devices. Figures 3a and b show EA/H_2/air premixed flame volumetric heat release rate at different H_2 concentrations and initial pressures, respectively. Figure 3a depicts that the amount of energy released from the combustion of the EA/H_2/air premixed flame increases when the concentration of H_2 in the fuel mixture increases. The maximum volumetric heat release rate at 0% of H_2 is

35.76 kW/cm^3, 4% of H_2 is 44.59 kW/cm^3, 8% of H_2 is 50.06 kW/cm^3, and 12% of H_2 is 57.70 kW/cm^3. Figure 3b shows that the volumetric heat release rate increases when the initial pressure increases. This implies a higher amount of energy is released from the combustion process when the initial pressure increases. The maximum volumetric heat release rate at 1 bar is 10.04 kW/cm^3, 2 bar is 31.02 kW/cm^3 and 3 bar is 57.70 kW/cm^3.

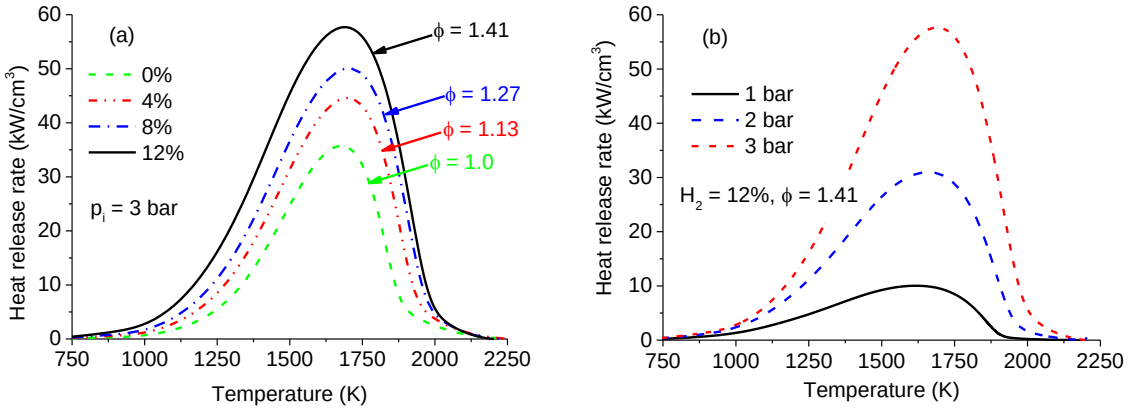


Fig. 3. Volumetric heat release rate at (a) different H_2 concentrations and (b) different initial pressures.

4.2. EA/H_2/air laminar burning speed

In Figure 4, the LBS study at H_2 of 4% is compared with the LBS of different fuel mixtures, n-hexane/H_2(40%) [10], EA/H_2(4%) [22], n-heptane/H_2(50%) [35], Ethanol/H_2(40%) [36], and methane/H_2(40%) [37] measured with the CVCC experimental set-up to validate this study's results. The findings of this study reveal a good trend with the LBS literature on the different fuels. Figure 5 shows the experimental and simulated LBS of EA/H_2/air at H_2 concentrations of 0-12% and pressures of 1-3 bar. The 0% data were obtained from Ref. [21]. The LBS increases with increasing H_2 concentration in the fuel mixture, as shown in Figures 5a-c, because hydrogen is a monatomic molecule with large thermal diffusivity due to its low specific heat and high thermal conductivity [38]. As the H_2 concentration in the fuel mixture increases, the adiabatic temperature and reactivity or reaction rate of the EA/H_2/air premixed flame increases, leading to increased LBS [36]. Also, the increase in the concentration of H_2 in the fuel mixture increases the concentration of active radicals in the EA/H_2/air premixed flame, which accelerates the reaction rate of the combustion and increases the LBS [39]. The magnitude of the LBS follows the order of 12% > 8% > 4% > 0%. Moreover, it is evident in Figures 5a-d that the simulated LBS correlates well with the experimental LBS. Therefore, the chemical mechanism

used for the simulation can give a good prediction or reproduce the LBS at the various investigated conditions. Figure 5d shows that the experiment and simulated LBS correlate well within an error of ±10%. Figures 6a-b show that the LBS decreases with increasing initial pressure due to increased burnt gas density and changes in important three-body chain termination reactions [40]. Finally, Table 1 provides the coefficients for the LBS correlation (Equation (11)) with the initial pressures.

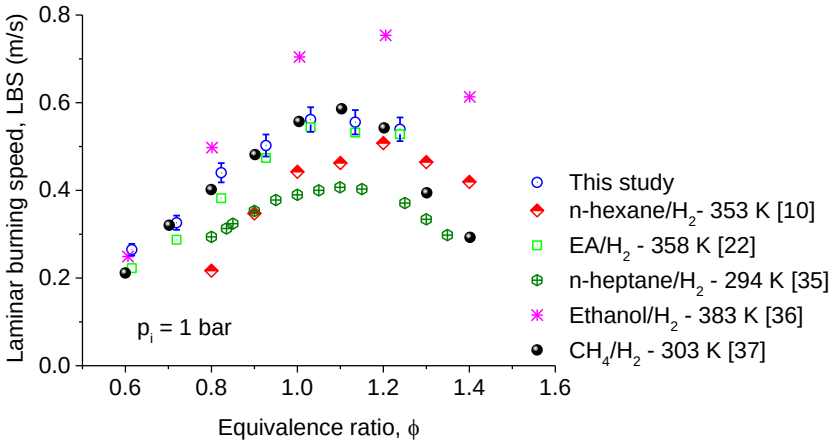
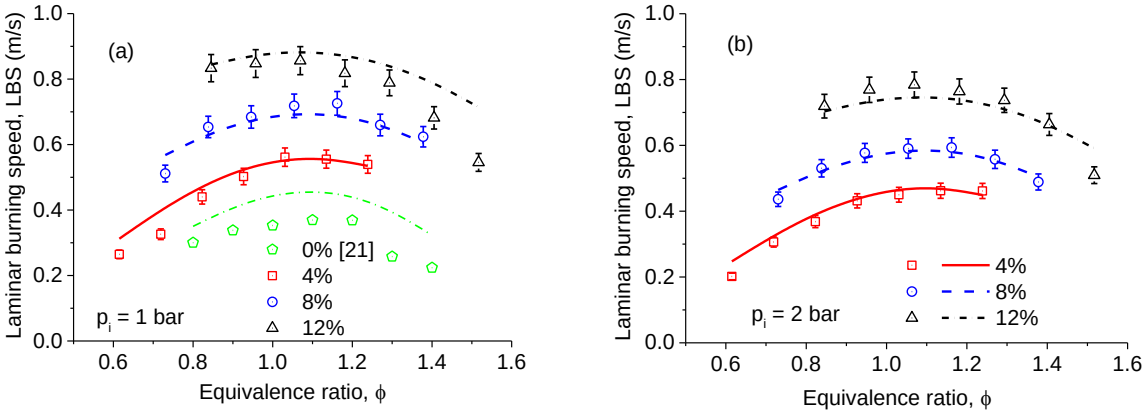
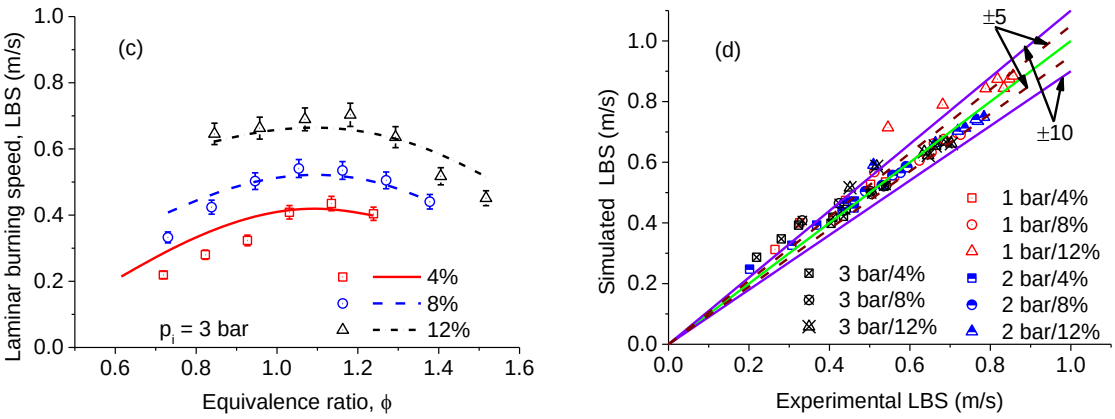
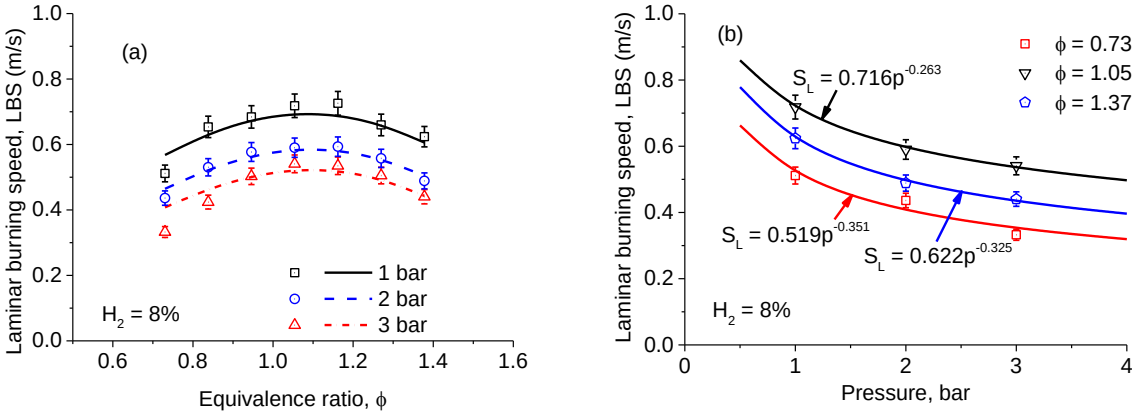


Fig. 4. EA/H_2/air and different fuels premixed flame LBS at 1 bar.





224 Fig. 5. EA/H_2/air LBS at 1-3 bar and H_2 of 0-12%. Symbols: Experiment and Lines: Simulation (Figs. 5a-c).



225 Fig. 6. Effects of initial pressure on LBS. Lines in (a) are simulations and (b) fittings correlations.

226

227 Table 1. Correlation data for S_L^0 and β data obtained at H_2 of 4-12%.

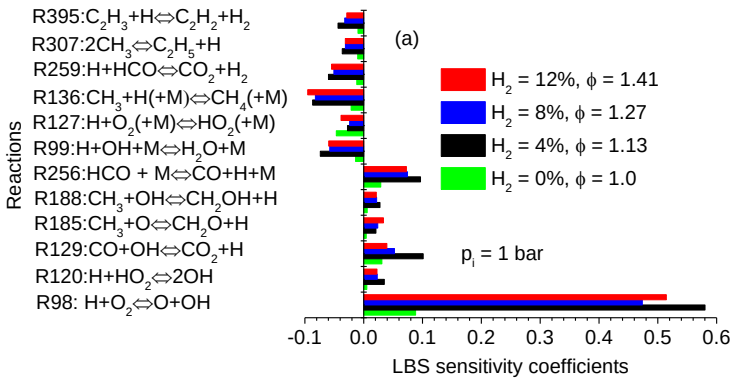
4%			8%			12%		
ϕ	S_L^0, m/s	a	ϕ	S_L^0, m/s	a	ϕ	S_L^0, m/s	a
0.61	0.265	-0.393	0.73	0.519	-0.351	0.84	0.835	-0.229
0.72	0.336	-0.297	0.84	0.659	-0.371	0.95	0.856	-0.207
0.82	0.447	-0.371	0.95	0.687	-0.273	1.06	0.864	-0.184
0.93	0.511	-0.355	1.05	0.719	-0.263	1.18	0.822	-0.131
1.03	0.559	-0.296	1.16	0.725	-0.280	1.29	0.799	-0.178
1.13	0.553	-0.231	1.27	0.659	-0.243	1.41	0.699	-0.208
1.24	0.542	-0.255	1.38	0.622	-0.325	1.52	0.551	-0.160

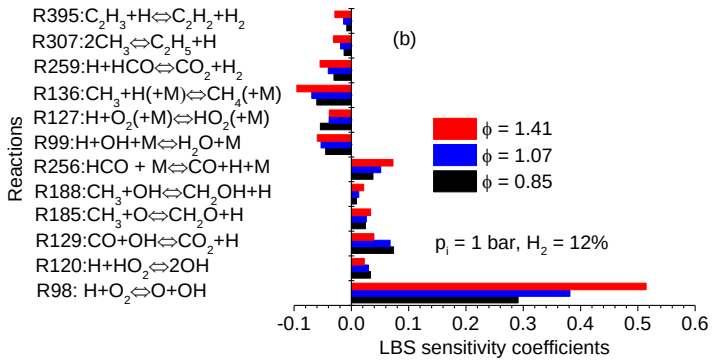
228 **4.3. EA/H_2/air sensitivity coefficient, rate of progress, production rate, and pathway analysis**

229 A sensitivity analysis of the flame speeds was performed to evaluate the combustion reaction that
230 significantly influences EA/H_2/air flame propagation. Figures 7a-c show the LBS sensitivity coefficients of
231 the EA/H_2/air premixed flame for different H_2 concentrations, equivalence ratios, and initial pressures.
232 According to the sensitivity analysis (see Figures 7a-c), reactions R98: H + O_2 ⟺ O + OH, R120: H + HO_2
233 ⟺ 2OH, R129: CO + OH ⟺ CO_2 + H, R185: CH_3 + O ⟺ CH_2O + H, R188: CH_3 + OH ⟺ CH_2OH + H,

and R256: HCO + M ⇔ CO + H + M have positive sensitivity coefficients and promote the reactivity of EA/H_2/air premixed flame. However, the chain branching reactions R98 and R256 and the exothermic reaction R129 significantly accelerate the flame speed. The chain branching reaction R98 generates an ample number of O and OH radicals, which increases EA/H_2/air reactivity and the flame speed more than R256. Strikingly, the exothermic reaction R129 significantly increases the flame temperature and speed.

On the contrary, the sensitivity coefficients of the reactions R99: H + OH + M ⇔ H_2O + M, R127: H + O_2(+M) ⇔ HO_2(+M), R136: CH_3 + H (+M) ⇔ CH_4 (+M), R259: H + HCO ⇔ CO_2 + H_2, R307: 2CH_3 ⇔ C_2H_5 + H, and R395: C_2H_3 + H ⇔ C_2H_2 + H are negative. Therefore, these reactions inhibit the reactivity of EA/H_2/air premixed flame. They consume the active radicals in the EA/H_2/air premixed flames and form stable radicals and species. Therefore, they decrease the reactivity of the EA/H_2/air premixed flame and decelerate the flame speed. Nonetheless, the termination or methyl specific reaction R136 significantly impedes EA/H_2/air premixed flame reactivity. Next to R136 is reaction R99 which competes with R98, decreases the production of H and OH radicals in the combustion process and impedes EA/H_2/air reactivity. In summary, radicals such as H, O, and OH produced during combustion increase combustion reactivity by acting as chain carriers, enhancing chain propagation, and increasing flame speed.





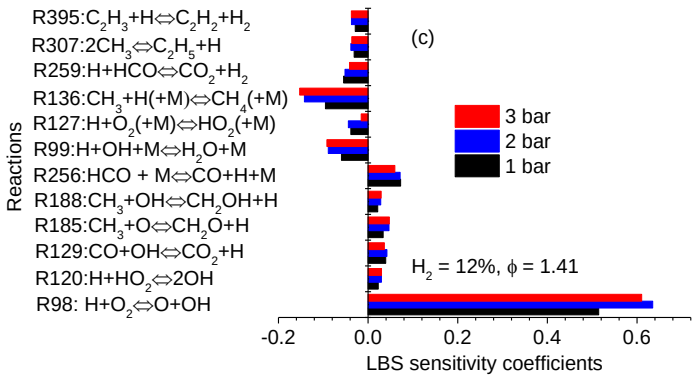
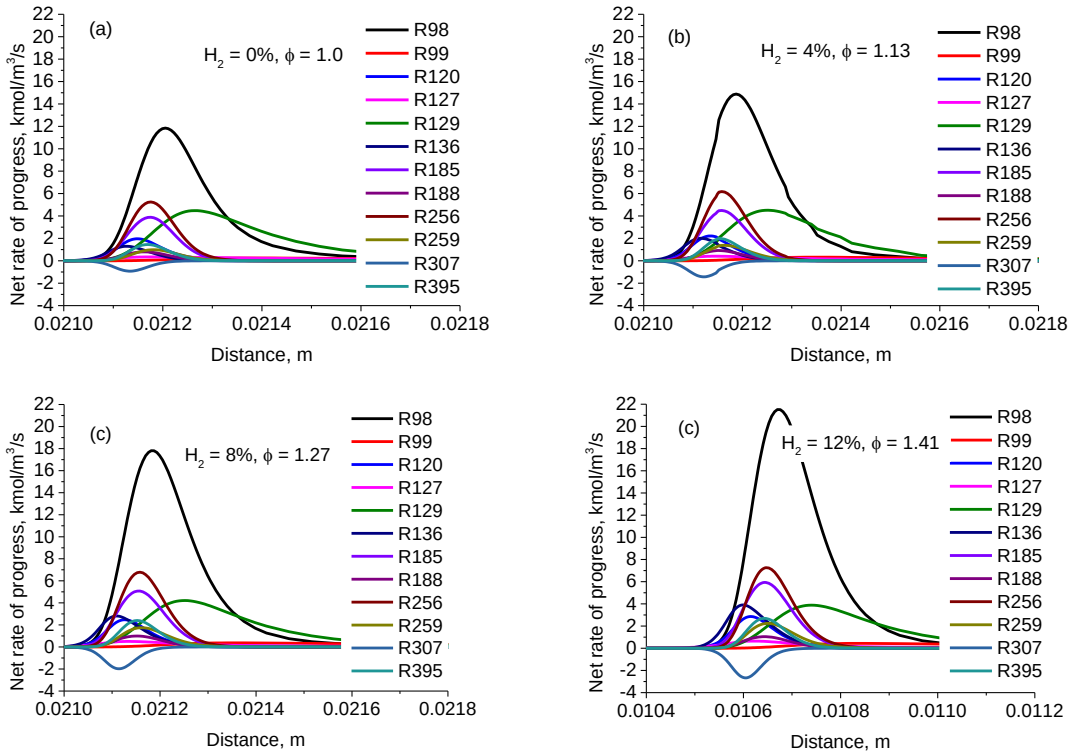


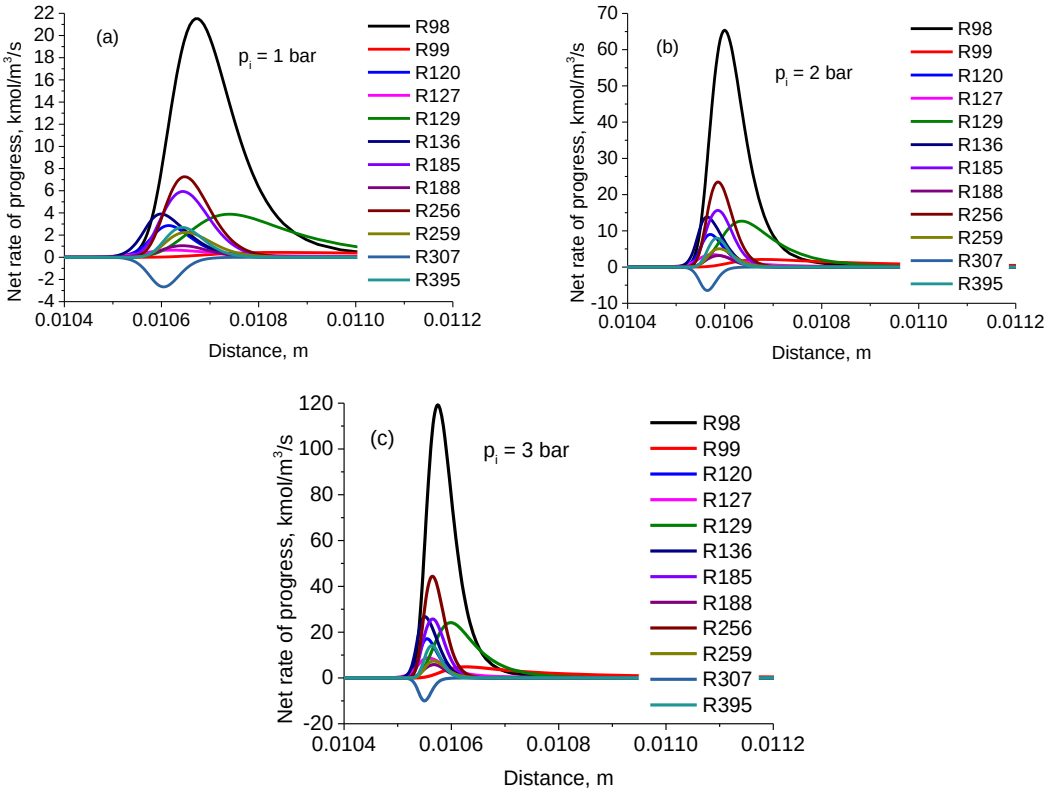
Fig. 7. EA/H_2/air LBS sensitivity coefficients at different (a) H_2 concentrations (b) equivalence ratios, and (c) initial pressures.

Moreover, Figures 8a-d and 9a-c show the net rate of progress of the topmost reactions of the EA/H_2/air premixed flame at different H_2 concentrations and initial pressures, respectively. As given in the figures, the reaction rate increases with increasing H_2 concentration and initial pressure. The premixture with an H_2 of 12% and a pressure of 3 bar has the maximum rate of progress. Again, Figures 8a-d and 9a-c show that R98 has the highest reaction rate, followed by R265, R185 and R129. Therefore, R98 significantly influences the reactivity of EA/H_2/air, i.e., R98 produces a lot of O and OH radicals, which serve as chain carriers in the combustion process to enhance the reactivity of EA/H_2/air. The maximum progress rate of R98 at H_2 of 0% is 11.84 kmol/m^3/s, 14.88 kmol/m^3/s at H_2 of 4%, 17.81 kmol/m^3/s at H_2 of 8%, and 21.52 kmol/m^3/s at H_2 of 12%. The maximum progress rate of R98 at 1 bar is 21.52 kmol/m^3/s, 2 bar is 65.37 kmol/m^3/s, and 3 bar is 119.24 kmol/m^3/s. Figures 10a-c also provide the production rates of some relevant species in the combustion phenomenon. As can be observed, the formation of H_2O is higher than the other species, followed by CO and CO_2 (see Figures 10a-c). EA and O_2 are mostly consumed in the combustion process, whereas H_2 is first produced and then consumed. Lastly, H is first consumed and then produced.



270 Fig. 8. Progression rate of EA/H_2/air premixed flame of main reactions at 1 bar and H_2 of 0-12%.

271



272 Fig. 9. Progression rate of EA/H_2/air premixed flame of main reactions at 1-3 bar, H_2 of 12% and ϕ = 1.41.

273

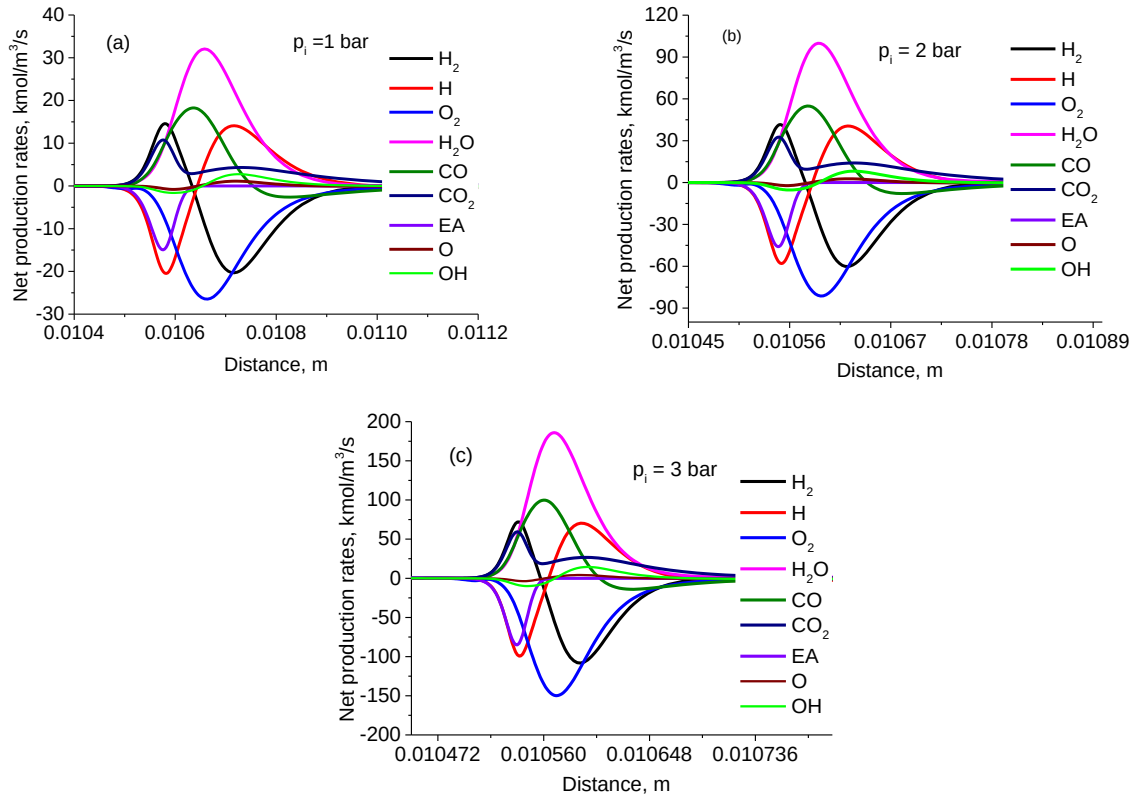
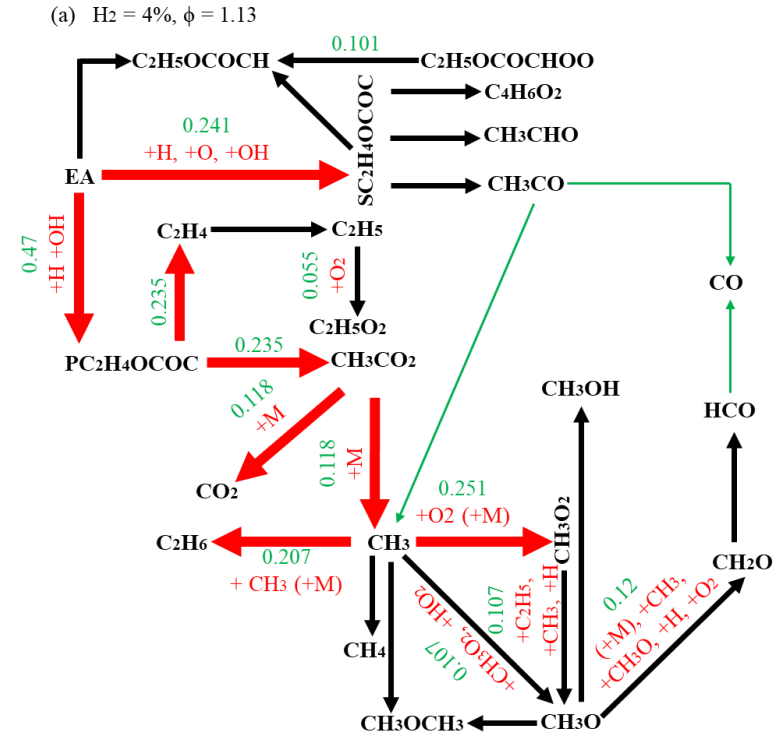


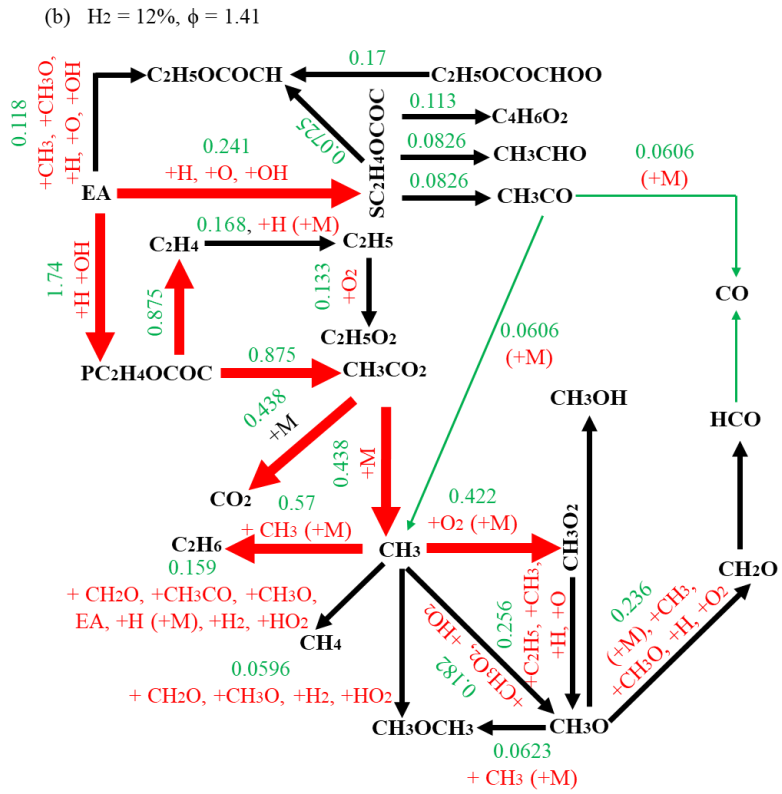
Fig. 10. Production rate of EA/H_2/air premixed flame relevant species at 1-3 bar, H_2 of 12% and ϕ = 1.41.

Figures 11a and b show the reaction pathway analysis of EA/H_2/air following the carbon (C) atom. The data represent the pathways of EA/H_2/air with H_2 concentrations of 4 and 12% at 1 bar, respectively. The reaction pathways of the EA/H_2/air premixed flames are determined at the maximum temperature gradient (acknowledged as the flame front whereby maximum heat is released) of the flame structure. As displayed in Figures 11a and b, H-abstraction is mainly responsible for the decomposition of EA. Figures 11a and b depict that the main pathway for converting EA to CO_2 is EA→PC_2H_4OCOC→CH_3CO_2(acetate)→CO_2. Thus, EA is attacked by +H and +OH radicals to produce PC_2H_4OCOC. Acetate(CH_3CO_2) is further formed from PC_2H_4OCOC and, finally, CO_2 is generated from CH_3CO_2. More so, the formation of CO is via EA decomposing into SC_2H_4OCOC and then into acetyl CH_3CO and oxidizing into CO. The other route for EA to CO is EA→PC_2H_4OCOC→CH_3CO_2(acetate)→CH_3(methyl)→CH_3O_2(hydroxymethoxide)→CH_3O(hydroxymethyl)→CH_2O(formaldehyde)→HCO→CO.EA→PC_2H_4OCOC→CH_3CO_2→CH_3→CH_3O_2→C_2H_6/CH_4/CH_3OCH_3 is another relevant pathway. Lastly, it can be seen from Figures 11a and b that more hydrogen atoms are formed when the concentration of hydrogen in the fuel mixture increases.



289

290



291

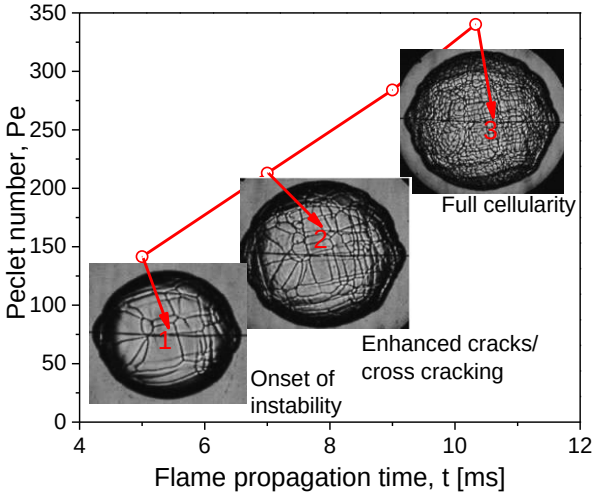
292 Fig. 11. Reaction pathways of EA/H_2/air premixed flame following a C atom. (a) 4% and (b) 12% at 1 bar.

293 The mole flux is represented by green colour and the radicals for the decomposition in red colour.

4.4. EA/H_2/air premixed flame intrinsic instability analysis

Thermal-diffusion instability (TD), hydrodynamic instability (Darrieus-Landau, DL), and instability due to buoyancy (Rayleigh-Taylor instability) are the main intrinsic instabilities prevalent in a premixed flame. TD instability is caused by non-equidiffusion (mostly determined in terms of the Lewis number) of the premixture [41]. The stretch rate of the premixed flame can also reinforce or weaken TD instability [42]. DL is caused by the thermal expansion of the premixed flame gases [11]. Moreover, attenuated flame thickness decreases the flame curvature, increases the baroclinic torque of the premixed flame, and increases DL instability [43]. Buoyancy instability occurs when the premixed flame is subjected to an acceleration field [44]. That is, the light burnt gas floats on top of the heavy unburnt gas or moves upwards due to buoyancy, and the heavy unburnt gas moves downwards due to gravity. Therefore, this motion destabilizes the premixed flame, and perturbations on the flame grow with time. In this study, only TD and DL instabilities were found in the EA/H_2/air premixed flame. These instabilities are presented and discussed.

Figure. 12 shows the evolution of EA/H_2/air premixed flame intrinsic instabilities. Panel 1 depicts the onset of flame cracks caused by TD [45,46]. As the combustion progresses, the non-equidiffusion or preferential diffusion of the premixture further causes the cracks to develop into enhanced cross/branch cracks as shown in panel 2. Besides, panel 3 shows full cellularity or an ample number of cells on the flame surface evoked by DL. As the flame radially expands, the flame thickness decreases due to increased pressure, and the stretch rate stabilization on the flame front surface decreases (thermal-diffusion stabilization declines). Therefore, the hydrodynamic instability intensity is strengthened, which leads to the generation of a cluster of cells on the flame front as shown in panel 3 [46,47]. Thus, the DL instability becomes stronger than TD, generating an abundant number of smaller cells on the flame front and wrinkling the flame front.



316

317 Fig. 12. Evolution of intrinsic instabilities at 3 bar, H_2 of 12% and ϕ of 1.18.

318

319 Figure 13 shows the effects of different H_2 concentrations on the EA/H_2/air premixed flame instability. It
320 can be seen that EA/H_2/air premixed flames are smooth and stable when H_2 is 4%. Furthermore, when H_2 is
321 8%, cracks appear on the flame surface from 5 to 13.33 ms and destabilize the flame. The flame
322 instability/cellularity is more pronounced when H_2 is 12% (see 11.67 and 13.33 ms). The thermal-diffusion
323 stabilization effect on EA/H_2/air flame surface is strong when H_2 is 4%, which reinforces the flame
324 stabilization intensity, but the thermal-diffusion stabilization effect dwindles as H_2 concentration increases
325 (H_2 of 8 and 12%) leading to a more noticeable flame instability/cellularity. Thus, with the increase in H_2
326 concentration, the molecular diffusion of the fuel mixture increases and enhances thermal-diffusion
327 instability. In summary, from Figure 13, the reduced flame thickness and Lewis number contribute to
328 EA/H_2/air premixed flame instability/cellularity when the concentration of H_2 in the premixture increases.
329 Moreover, Figure 14 displays the effect of initial pressure on the instability/cellularity of EA/H_2/air
330 premixed flames. As observed, long length cracks appear on the EA/H_2/air flame surface at the propagation
331 times of 8.33-13.33 ms when the initial pressure is 1 bar. However, the EA/H_2/air flame becomes more
332 unstable, cellularized, and wrinkled when the initial pressure is 2 and 3 bar. Thus, as the initial pressure
333 increases, the EA/H_2/air flame thickness reduces, the EA/H_2/air flame stretch and curvature stabilization
334 strength decrease, and the baroclinic torque of the EA/H_2/air flame front also increases. Therefore, thermal-
335 diffusion stabilization reinforcement on the EA/H_2/air flame front decreases and hydrodynamic instability
336 destabilizes, cellularizes, and wrinkles EA/H_2/air premixed flames. In summation, Figure 14 shows that

increased thermal expansion ratio and decreased flame thickness significantly cause the instability/cellularity of EA/H_2/air premixed flames when the initial pressure increases.

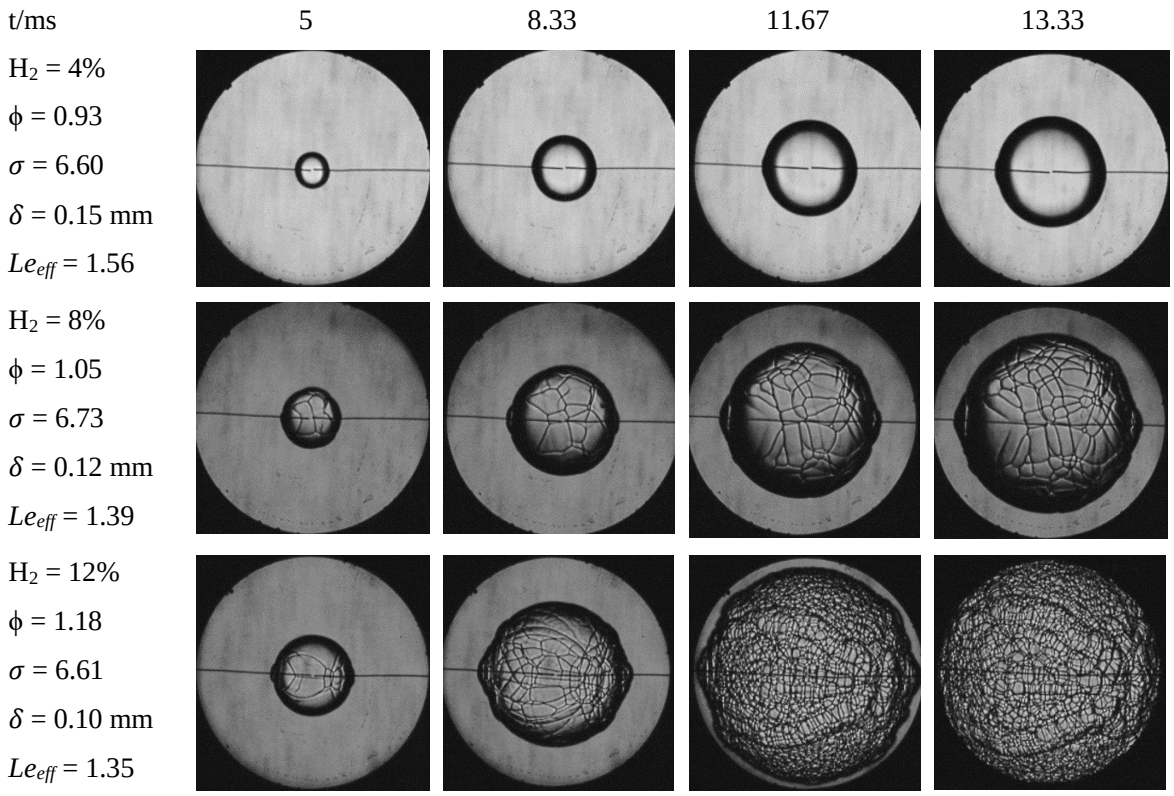
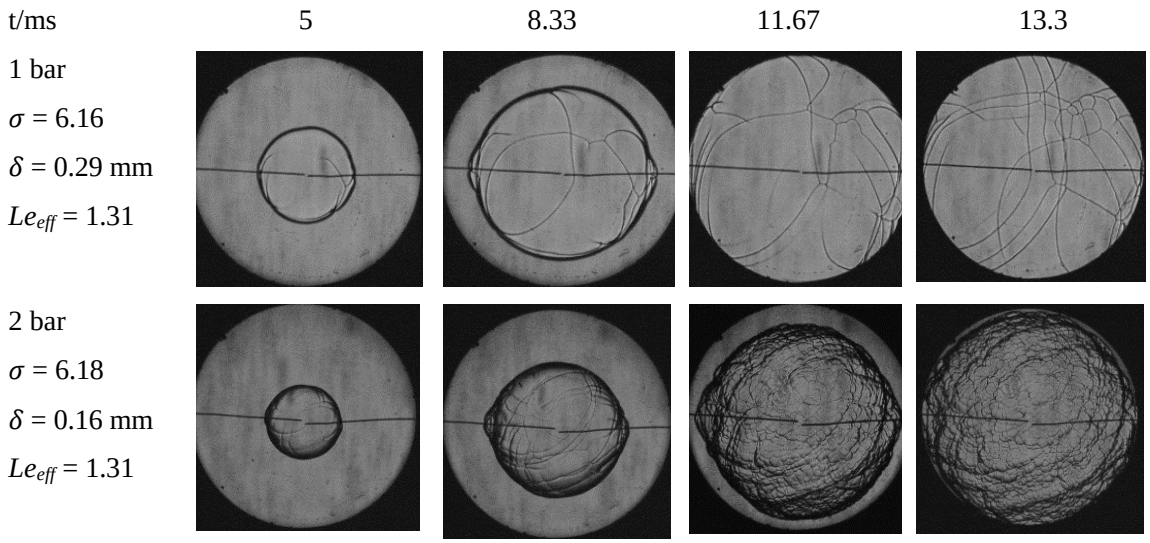


Fig. 13. EA/H_2/air premixed flame morphology at the initial pressure of 3 bar.



3 bar
σ = 6.20
δ = 0.11 mm
Le_{eff} = 1.51

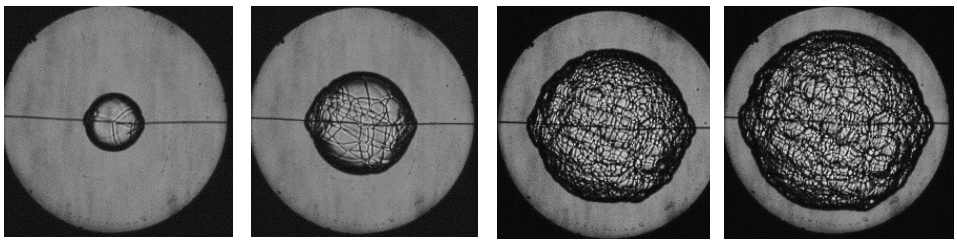


Fig. 14. EA/H_2/air premixed flame morphology at initial pressures of 1-3 bar, H_2 of 12%, and ϕ of 0.85.

Figure 15 shows the physicochemical properties that influence EA/H_2/air premixed flame instability presented in Figures 13 and 14 at different H_2 concentrations and the pressure of 3 bar. The effective Lewis number is presented in Figure 15a, whereas Figure 15b depicts the flame thickness of the EA/H_2/air premixed flame. Figure 15c illustrates the plot of the thermal expansion ratio of the EA/H_2/air premixed flame. The Lewis number determines the thermal-diffusion instability contribution to premixed flame instability. It quantifies the non-equidiffusion of the premixed flame. The flame is thermal-diffusively stable for premixtures with Lewis numbers greater than unity and unstable for premixtures with Lewis numbers less than unity. So, as the Lewis number decreases, the EA/H_2/air premixed flame instability and cellularity propensity increase. From Figure 15a, as is the case generally, the Lewis number of EA/H_2/air fuel mixture decreases with increasing H_2 concentration at lean to slightly rich mixtures due to increased molecular/mass diffusion of the premixture. Therefore, instability will occur early at these sides of the mixture [48,49]. Conversely, in rich mixtures, the molecular diffusion of the fuel mixture decreases with increasing H_2 concentration, leading to increased Lewis numbers and delayed onset of instability. Also, when the equivalence ratio decreases, the Lewis number decreases. Therefore, thermal-diffusion instability propensity increases. Finally, while the tendency for EA/H_2/air instability increases with decreasing Lewis number, the Lewis numbers of EA/H_2/air are greater than unity in this study. Therefore, EA/H_2/air premixed flames are thermal-diffusively stable.

Similarly, the flame thickness and thermal expansion ratio also characterize and quantify the hydrodynamic instability of a premixed flame. The thinner the flame and the larger the thermal expansion ratio, the higher the domineering power of hydrodynamic instability on the premixed flame. As seen from Figure 15b, EA/H_2/air premixed flame thickness decreases when H_2 concentration increases, thereby, enhancing hydrodynamic instability propensity. The reduction in the flame thickness decreases the flame curvature and increases the density and pressure gradient (baroclinic torque) within the EA/H_2/air premixed

flame. Therefore, the flame susceptibility to hydrodynamic instability increases. Lastly, Figure 15c shows that the thermal expansion ratio decreases when the concentration of H_2 in the fuel mixture increases, indicating that hydrodynamic instability is inhibited when the H_2 concentration in the EA/H_2/air premixture increases.

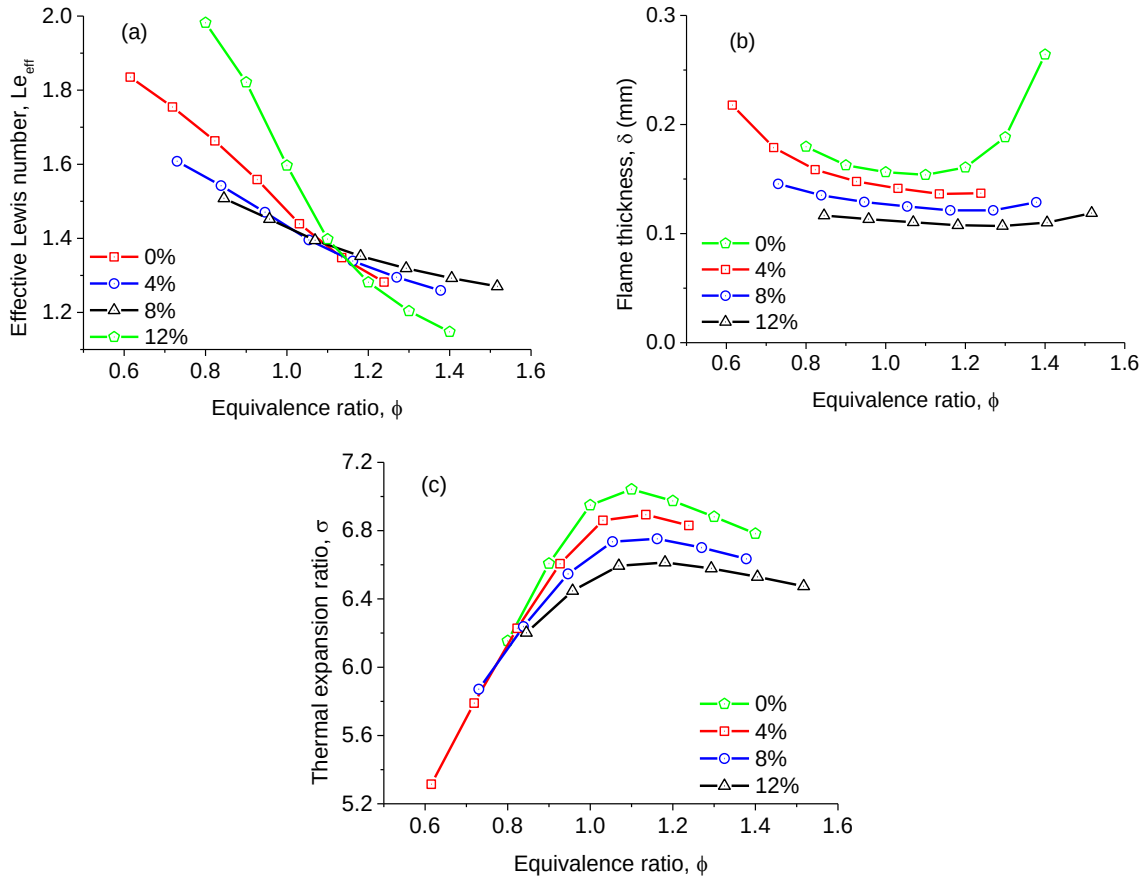


Fig. 15. EA/H_2/air (a) effective Lewis number, (b) flame thickness, and (c) thermal expansion ratio at the initial pressure of 3 bar and H_2% of 0-12%.

The theoretical analysis of the EA/H_2/air premixed flames is presented in Figures 16 and 17, while Figure 18 compares the theoretical and experimental instability analysis. Figure 16 illustrates the plot of the stability/peninsular-like curves of EA/H_2/air premixed flames. Following Addabbo et al. [50] the peninsular-like or stability curves were obtained using Equation (16).

$$Pe = \frac{\Omega(\sigma, \mathrm{Pr}, \mathrm{n}, Le_{eff})}{\omega(\mathrm{n}, \sigma)} \quad (16)$$

The thermal-diffusion effect of instability (Ω) is:

$$\Omega = \Omega_1 + \Omega_2 \frac{\beta(Le_{eff} - 1)}{\sigma - 1} + \Omega_3 Pr \quad (17)$$

The hydrodynamic effect of instability (ω) is:

$$\omega = \frac{-(b-a) + \sqrt{(b-a)^2 - 4ac}}{2a} \quad (18)$$

Whereas Ω depends on the thermal expansion ratio, Prandtl number, wavenumber, and Lewis number ω solely depend on the thermal expansion ratio and wavenumber. Ω_1, Ω_2, and Ω_3 are the heat conduction, molecular diffusion and viscous effects coefficients respectively. $Pr = \mu c_p/\lambda_{th}$ is the Prandtl number of the premixed flame. μ, c_p and λ_{th} are the dynamic viscosity, specific heat capacity at constant pressure, and thermal conductivity, respectively. Readers should refer to Beeckmann et al. [51] for the definitions of Ω_1, Ω_2, Ω_3, a, and b.

Figure 16a displays the stability curves at different equivalence ratios of 0.85 to 1.52 whilst, Figure 16b shows the stability curves for different H_2 concentrations of 0%, 4%, 8%, and 12%. The nose of the peninsular curve represents the critical conditions for the onset of instability, that is, the critical wavenumber (n_c) and the Peclet number (Pe_c). As observed in Figure 16a, the onset of instability occurs earlier in rich mixtures than in lean mixtures, whereas in Figure 16b, the onset of instability is early for the fuel mixture with an H_2 concentration of 12%. When the concentration of H_2 in the fuel mixture increases the molecular diffusion of the fuel mixture also increases. This increases the preferential diffusion of the premixture, causing early onset of instability. The onset of instability follows the order of 12% > 8% > 4% > 0%.

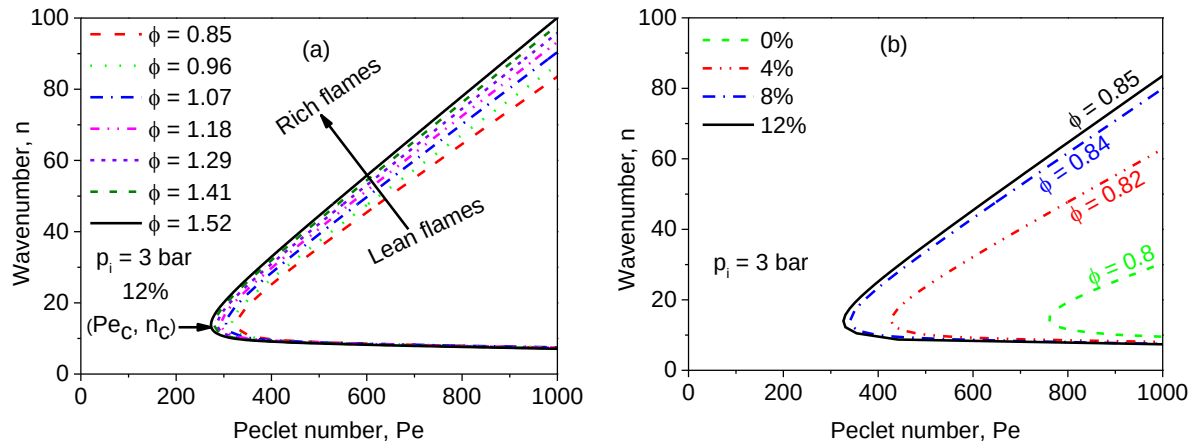


Fig. 16. Peninsula curves for different (a) equivalence ratios and (b) H_2 concentrations at 3 bar.

As presented in Figure 17, whereas the hydrodynamic effect of growth rate (ω) destabilizes EA/H_2/air flame at all the equivalence ratios, the thermal-diffusion effect of growth rate (Ω) stabilizes EA/H_2/air flame at all the equivalence ratios for the respective H_2 concentrations. Overall, the EA/H_2/air flame is unstable at all the equivalence ratios when the H_2 concentration is 8 or 12%. This is due to the higher propensity of hydrodynamic effects of growth rate to overpower the thermal-diffusion effects of growth rate [34]. However, the EA/H_2/air flame is stable for $\phi \leq 0.82$ but unstable for $\phi > 0.82$ when the H_2 concentration in the premixture is 4%. The flame is stable (unstable) when the perturbation growth rate in Figure 17 is negative (positive). The perturbation growth rate in Figure 17 was determined using $\Sigma = (\omega - \Omega Pe^{-1})$ at a wavenumber of 13.9 and a Peclet number of 400.

The plots of the critical Peclet number (Pe_c) for EA/H_2/air premixture with H_2 concentrations of 8% and 12%, respectively are shown in Figures 18a and b. It is worth noting that the experimental Peclet numbers were determined at a point when the flame surface was covered with enough cells [52]. Whereas the experimental critical Peclet numbers were computed using $Pe_c = R_c/\delta$ the theoretical Peclet numbers were calculated using Equation (16). R_c is the critical flame radius. Inferring from Figure 18a, the experimental critical Peclet numbers are usually higher than the theoretical values. This is indicative of the insignificant effect of lower concentration of the H_2 on the earlier onset of instability. However, in Figure 18b, flame instability appears early at lean mixtures to slightly rich mixtures in the experiment. This could be ascribed to increased molecular diffusion when the H_2 concentration of 12% is added to the fuel mixture. Other factors that could contribute to the discrepancies between the experimental and theoretical critical Peclet numbers in Figures 18a and b is the uncertainties in calculating parameters like the activation energy, Zel'dovich number,

Lewis number, flame thickness, etc. involved in the theoretical analysis [31,53]. More so, the accuracy of the chemical mechanism and underlying assumptions in the theory can also influence the disparities between the experimental and theoretical Peclet numbers [54]. Similar observations have been made in the literature for different fuels [31,53].

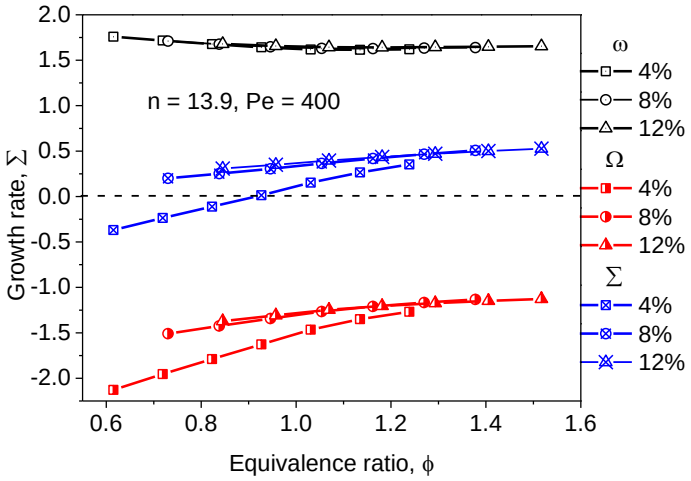


Fig. 17. EA/H_2/air premixed flame growth rate for different H_2 concentrations at 3 bar.

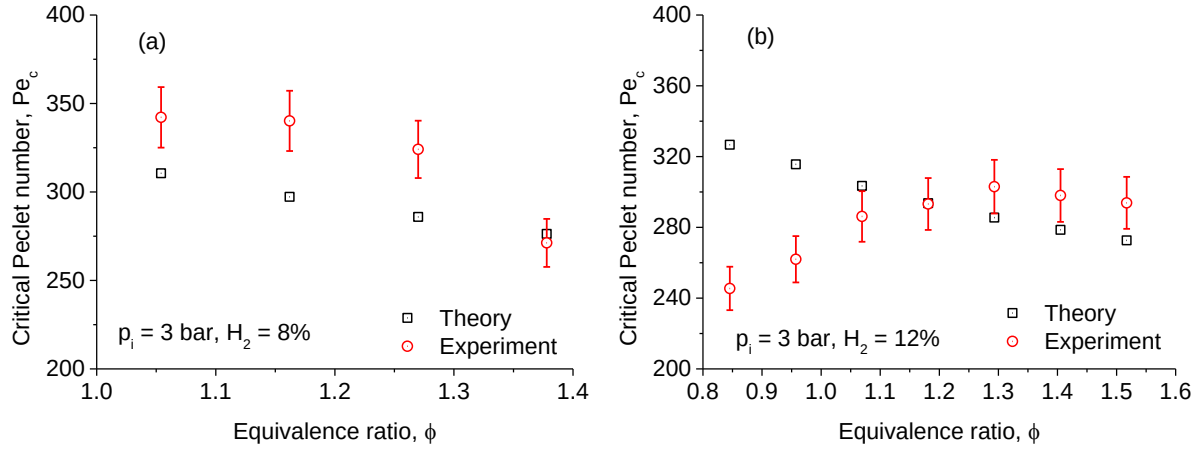


Fig. 18. EA/H_2/air premixed flame critical Peclet number at 3 bar for H_2 concentration of 8% and 12%. The experimental uncertainty is quantified with the 95% confidence interval.

5. Conclusions

This study investigated EA/H_2/air premixed flame laminar burning characteristics like laminar burning speed (LBS), intrinsic instability, etc. The investigations were conducted at the test conditions of 1 bar, 2 bar, and 3 bar and 358 K using hydrogen in air volumetric fractions of 0%, 4%, 8%, and 12% in a constant volume

combustion chamber. The constant volume method was used to determine the laminar burning speeds. Moreover, the experimental burning speeds were compared with the burning speeds obtained with the 1D freely propagating flame code in Cantera thermochemical software. The adiabatic flame temperature, thermal diffusivity, and heat release rate of the EA/H_2/air premixed flame were evaluated to assess the effect of H_2 on EA/H_2/air laminar flame dynamics. Also, chemical kinetics analysis was conducted to investigate the laminar burning speed sensitivity coefficients, the rate of progress of the main reactions, the production rate of relevant combustion species, and the reaction pathways of the EA/H_2/air premixed flame. The flame morphology, physicochemical properties, stability curves, growth rates, and critical Peclet numbers were used to examine EA/H_2/air premixed flame intrinsic instabilities. The main conclusions of this study are summarized below:

1. At the initial pressure of 1 bar, the maximum LBSs of 0.56 m/s, 0.72 m/s, and 0.85 m/s were measured for H_2 of 4%, 8% and 12%, respectively. The maximum LBSs at the initial pressure of 2 bar were 0.46 m/s, 0.59 m/s and 0.78 m/s for H_2 of 4%, 8% and 12%, respectively while the maximum LBSs of 0.43 m/s, 0.54 m/s and 0.70 m/s were measured at the initial pressure of 3 bar for H_2 of 4%, 8%, and 12%. The simulated burning speeds correlated well with the experimental burning speeds.

2. Reaction R98: $H + O_2 \Leftrightarrow O + OH$ produced a lot of O and OH radicals and promoted the reactivity of EA/H_2/air premixed flame. The termination reaction R136: $CH_3 + H (+M) \Leftrightarrow CH_4 (+M)$ significantly reduced the active radicals in the combustion process and decelerated EA/H_2/air premixed flame speed. The main pathway for the oxidation of EA to CO_2 was $EA \rightarrow PC_2H_4OCOC \rightarrow CH_3CO_2 \rightarrow CO_2$.

3. EA/H_2/air premixed flame was more prone to hydrodynamic instability when the concentration of H_2 in the fuel mixture and the initial pressure increased due to reduced flame thickness. The stability curves showed that EA/H_2/air premixed flame instability occurred early in premixed flames with a higher concentration of H_2. A comparison of the experimental and theoretical critical Peclet numbers indicated that EA/H_2/air flame instability was early in lean mixtures to slightly rich mixtures for fuel mixtures with 12% of H_2 in the experiment.

To sum up, the results of this study can be useful to combustion and energy engineers and related engineering discipline experts for the analysis, design, and optimization of energy conversion devices for the practical use of EA/H_2 fuel mixtures.

Acknowledgements

Thanks to the National Key R&D Program of China (No. 2018YFB1501405), Ningbo Major Science and Technology Project (20212ZDYF020041), Open Project of the State Key Laboratory of Clean Energy Utilization, Zhejiang University (ZJU-CEU2020001), and the China Postdoctoral Science Foundation for their support.

Reference

[1] Dabbagh HA, Ghobadi F, Ehsani MR, Moradmand M. The influence of ester additives on the properties of gasoline. Fuel 2013;104:216–23.

[2] Dayma G, Halter F, Foucher F, Mounaim-Rousselle C, Dagaut P. Laminar burning velocities of C_4–C_7 ethyl esters in a spherical combustion chamber : Experimental and detailed kinetic modeling. Energy and Fuels 2012;26:6669–77.

[3] Amine M, Awad EN, Ibrahim V, Barakat Y. Effect of ethyl acetate addition on phase stability, octane number and volatility criteria of ethanol-gasoline blends. Egypt J Pet 2018;27:567–72.

[4] Çakmak A, Kapusuz M, Özcan H. Experimental research on ethyl acetate as novel oxygenated fuel in the spark-ignition (SI) engine. Energy Sources, Part A Recover Util Environ Eff 2020:1–16.

[5] Contino F, Foucher F, Mounaïm-Rousselle C, Jeanmart H. Experimental characterization of ethyl acetate, ethyl propionate, and ethyl butanoate in a homogeneous charge compression ignition engine. Energy and Fuels 2011;25:998–1003.

[6] Xie Y, Sun ZY. Effects of the external turbulence on centrally- ignited spherical unstable CH_4/H_2/air flames in the constant-volume combustion bomb. Int J Hydrogen Energy 2019;44:20452–61.

[7] Di Sarli V, Di Benedetto A. Laminar burning velocity of hydrogen-methane/air premixed flames. Int J Hydrogen Energy 2007;32:637–46.

[8] Cammarota F, Di Benedetto A, Di Sarli V, Salzano E, Russo G. Combined effects of initial pressure and turbulence on explosions of hydrogen-enriched methane/air mixtures. J Loss Prev Process Ind 2009;22:607–13.

[9] Emami SD, Rajabi M, Hassan CRC, Hamid MDA, Kasmani RM, Mazangi M. Experimental study on premixed hydrogen/air and hydrogen-methane/air mixtures explosion in 90 degree bend pipeline. Int J Hydrogen Energy 2013;38:14115–20.

[10] Zhang L, Ma H, Pan J, Shen Z, Wang L, Liu R, et al. Effects of hydrogen addition on the explosion characteristics of n-hexane/air mixtures. Int J Hydrogen Energy 2019;44:2029–38.

[11] Williams FA. Combustion theory: The fundamental theory of chemically reacting flow systems, second edition. Second Edi. The Benjamin/Cummings Publishing Company, Inc; 1985.

[12] Konnov AA, Mohammad A, Kishore VR, Kim N Il, Prathap C, Kumar S. A comprehensive review of measurements and data analysis of laminar burning velocities for various fuel+air mixtures. Prog Energy Combust Sci 2018;68:197–267.

[13] Oppong F, Xu C, Li X, Zhongyang L. Laminar flame characteristics of 2-ethylfuran/air mixtures: Experimental and kinetic modelling investigations. Fuel 2022;307:121785.

[14] Mitu M, Razus D, Schroeder V. Laminar burning velocities of hydrogen-blended methane-air and natural gas–air mixtures, calculated from the early stage of p(t) records in a spherical vessel. Energies 2021;7556:1–16.

[15] Mitu M, Razus D, Giurcan V, Oancea D. Normal burning velocity and propagation speed of ethane-air: Pressure and temperature dependence. Fuel 2015;147:27–34.

[16] Cracknell R, Head B, Remmert S, Wu Y, Prakash A, Luebbers M. Laminar burning velocity as a fuel characteristic: Impact on vehicle performance. Intern. Combust. Engines Performance, Fuel Econ. Emiss. IMechE, London, 27-28 Novemb. 2013, 2013, p. 149–56.

[17] Kim G, Almansour B, Terracciano AC, Park S, Vasu SS. Laminar burning velocity measurements in methyl ester/air mixtures. AIAA Scitech 2019 Forum 2019:1–6.

[18] Badawy T, Williamson J, Xu H. Laminar burning characteristics of ethyl propionate, ethyl butyrate, ethyl acetate, gasoline and ethanol fuels. Fuel 2016;183:627–40.

[19] Nilsson EJK, Konnov AA. Trends in laminar burning velocities of C_2-C_7 esters. Proc Eur Combust Meet 2015:5–8.

[20] Ahmed A, Pitz WJ, Cavallotti C, Mehl M, Lokachari N, Nilsson EJK, et al. Small ester combustion chemistry: Computational kinetics and experimental study of methyl acetate and ethyl acetate. Proc Combust Inst 2019;37:419–28.

[21] Oppong F, Zhongyang L, Li X, Xu C. Investigations on laminar premixed flame characteristics of ethyl acetate. Combust Flame 2021;230:111454.

[22] Xu C, Wu S, Oppong F, Xie C, Wei L, Zhou J. Experimental and numerical studies of laminar flame characteristics of ethyl acetate with or without hydrogen addition. Int J Hydrogen Energy 2020;45:20391–9.

[23] Oppong F, Zhongyang L, Li X, Xu C. Inherent instabilities in ethyl acetate premixed flames. Fuel 2021;290:120000.

[24] Luijten CCM, Doosje E, de Goey LPH. Accurate analytical models for fractional pressure rise in constant volume combustion. Int J Therm Sci 2009;48:1213–22.

[25] Faghih M, Chen Z. The constant-volume propagating spherical flame method for laminar flame speed measurement. Sci Bull 2016;61:1296–310.

[26] Razus D, Brinzea V, Mitu M, Movileanu C, Oancea D. Burning velocity of propane-air mixtures from pressure-time records during explosions in a closed spherical vessel. Energy and Fuels 2012;26:901–9.

[27] Chen Z, Burke MP, Ju Y. Effects of compression and stretch on the determination of laminar flame speeds using propagating spherical flames. Combust Theory Model 2009;13:343–64.

[28] Goodwin DG, Moffat HK, Speth RL. Cantera: An Object-oriented Software Toolkit for Chemical Kinetics, Thermodynamics, and Transport Processes. 2017.

[29] Bechtold JK, Matalon M. The dependence of the Markstein length on stoichiometry. Combust Flame 2001;127:1906–13.

[30] Dinkelacker F, Manickam B, Muppala SPR. Modelling and simulation of lean premixed turbulent methane/hydrogen/air flames with an effective Lewis number approach. Combust Flame 2011;158:1742–9.

[31] Jomaas G, Law CK, Bechtold JK. On transition to cellularity in expanding spherical flames. J Fluid Mech 2007;583:1–26.

546 [32] Bradley D, Sheppart CGW, Woolley R, Greenhalgh DA, Lockett RD. The development and structure of
547 flame instabilities and cellularity at low Markstein numbers in explosions. Combust Flame 2000;122:195–
548 209.
549 [33] Stephen R Turns. An introduction to combustion : Concepts and applications. Third Edit. McGraw Hill;
550 2012.
551 [34] Glassman I, Yetter RA, Glumac NG. Combustion. Fifth Edit. Elsevier Ltd; 2015.
552 [35] Comandini A, Chaumeix N, Maclean JD, Ciccarelli G. Combustion properties of n-heptane/hydrogen
553 mixtures. Int J Hydrogen Energy 2019;44:2039–52.
554 [36] Li G, Zhang Z, Liang J, Dong F, Li Y, Gao X. Effects of hydrogen addition on the premixed laminar-
555 flames of ethanol e air gaseous mixtures : An experimental study. Int J Hydrogen Energy 2011;37:4490–
556 501.
557 [37] Hu E, Huang Z, He J, Jin C, Zheng J. Experimental and numerical study on laminar burning characteristics
558 of premixed methane-hydrogen-air flames. Int J Hydrogen Energy 2009;34:4876–88.
559 [38] Ueda A, Nisida K, Matsumura Y, Ichikawa T, Nakashimada Y, Endo T, et al. Effects of hydrogen and
560 carbon dioxide on the laminar burning velocities of methane-air mixtures. J Energy Inst 2021;99:178–85.
561 [39] Tang C, He J, Huang Z, Jin C, Wang J, Wang X, et al. Measurements of laminar burning velocities and
562 Markstein lengths of propane-hydrogen-air mixtures at elevated pressures and temperatures. Int J
563 Hydrogen Energy 2008;33:7274–85.
564 [40] Law CK. Combustion Physics. First Edit. Cambridge University Press; 2006.
565 [41] Lapalme D, Halter F, Mounaïm-Rousselle C, Seers P. Characterization of thermodiffusive and
566 hydrodynamic mechanisms on the cellular instability of syngas fuel blended with CH_4 or CO_2. Combust
567 Flame 2018;193:481–90.
568 [42] Bradley D. Instabilities and flame speeds in large-scale premixed gaseous explosions. Philos Trans R Soc
569 A Math Phys Eng Sci 2000;358:3567–81.
570 [43] Wu F, Jomaas G, Law CK. An experimental investigation on self-acceleration of cellular spherical flames.
571 Proc Combust Inst 2013;34:937–45.
572 [44] Clavin P. Dynamic behavior of premixed flame fronts in laminar and turbulent flows. Prog Energy
573 Combust Sci 1985;11:1–59.

574 [45] Thimothée R, Chauveau C, Halter F, Gökalp I. Experimental investigation of the mechanisms of cellular
575 instabilities developing on spherical two-phase flames. Combust Sci Technol 2016;188:2026–43.
576 [46] Kim W, Endo T, Mogi T, Kuwana K, Dobashi R. Wrinkling of large-scale flame in lean propane-air
577 mixture due to cellular instabilities. Combust Sci Technol 2019;191:491–503.
578 [47] Karlin V, Sivashinsky G. Asymptotic modelling of self-acceleration of spherical flames. Proc Combust
579 Inst 2007;31 I:1023–30.
580 [48] Okafor EC, Nagano Y, Kitagawa T. Experimental and theoretical analysis of cellular instability in lean
581 H_2-CH4-air flames at elevated pressures. Int J Hydrogen Energy 2016;41:6581–92.
582 [49] Addabbo R. The structure and stability of expanding and converging near-stoichiometric flames. New
583 Jersy Institute of Technology, 2001.
584 [50] Addabbo R, Bechtold JK, Matalon M. Wrinkling of spherically expanding flames. Proc Combust Inst
585 2002;29:1527–35.
586 [51] Beeckmann J, Hesse R, Kruse S, Berens A, Peters N, Pitsch H, et al. Propagation speed and stability of
587 spherically expanding hydrogen/air flames: Experimental study and asymptotics. Proc Combust Inst
588 2017;36:1531–8.
589 [52] Bradley D, Cresswell TM, Puttock JS. Flame acceleration due to flame-induced instabilities in large-scale
590 explosions. Combust Flame 2001;124:551–9.
591 [53] Kwon OC, Rozenchan G, Law CK. Cellular instabilities and self-acceleration of outwardly propagating
592 spherical flames. Proc Combust Inst 2002;29:1775–83.
593 [54] Law CK, Jomaas G, Bechtold JK. Cellular instabilities of expanding hydrogen/propane spherical flames
594 at elevated pressures : theory and experiment 2005;30:159–67.
595